

# 1 Spage2vec: Unsupervised detection of spatial gene 2 expression constellations

3 Gabriele Partel\*<sup>1</sup>, and Carolina Wählby\*<sup>1</sup>

4

5 1. Centre for Image Analysis, Dept. of Information Technology and SciLifeLab,  
6 Uppsala University, Uppsala, Sweden

7 \* Correspondence: [gabriele.partel,carolina.wahlby@it.uu.se](mailto:gabriele.partel,carolina.wahlby@it.uu.se)

8

## 9 ABSTRACT

10 Investigation of spatial cellular composition of tissue architectures revealed by multiplexed in situ RNA  
11 detection often rely on inaccurate cell segmentation or prior biological knowledge from complementary  
12 single cell sequencing experiments. Here we present spage2vec, an unsupervised segmentation free  
13 approach for decrypting the spatial transcriptomic heterogeneity of complex tissues at subcellular  
14 resolution. Spage2vec represents the spatial transcriptomic landscape of tissue samples as a spatial  
15 functional network and leverages a powerful machine learning graph representation technique to  
16 create a lower dimensional representation of local spatial gene expression. We apply spage2vec to  
17 mouse brain data from three different in situ transcriptomic assays, showing that learned  
18 representations encode meaningful biological spatial information of re-occurring gene constellations  
19 involved in cellular and subcellular processes.

20

## 21 INTRODUCTION

22 Recent advances in single-cell RNA (scRNA) sequencing [1,2] allow to dissect the cell type  
23 heterogeneity of complex tissues at incredible pace. An international effort has started building  
24 comprehensive reference maps of gene expression at cellular resolution to uncover the cell type  
25 composition of entire organs and organisms [3]. However, in order to understand the functional  
26 architecture of a tissue it is essential to reconstruct the spatial organization of its constituent cell

27 types. To this end, single cell sequencing analyses are often complemented with imaging-based  
28 methods for spatially resolved multiplexed in situ RNA detection [4-8] that allow to map mRNA  
29 molecules directly in tissue samples and identify specific cell type location, enabling the discovery of  
30 their functional role inside the tissue architecture.

31  
32 Previous attempts to map the spatial heterogeneity of cell types mostly relied on cell body  
33 segmentation algorithms and gene assignments to cells based on segmented cell boundaries [4-7].  
34 Extracted per-cell gene expression profiles are successively clustered and annotated based on  
35 complementary scRNA sequencing analysis experiments or published literature [4-7].  
36 This means that analysis of the spatial heterogeneity in tissue samples is limited by the accuracy of  
37 image segmentation algorithms to outline exact cell borders in dense and overlapping cell  
38 environments, with uneven illumination conditions and low-signal to noise ratios. Moreover, while  
39 some cell types are defined by clear differences in their gene expression profiles, others differ by only  
40 a few genes in their transcriptome (e.g. like finely related neuronal subtypes) making their  
41 identification challenging.

42  
43 Preliminary work from *Park J, Choi W. et al.* [9] tries to address these problems proposing a  
44 segmentation-free spatial cell-type analysis (SSAM) based on cellular mRNA density estimation via  
45 Gaussian KDE [10], defining cell location as local maxima of mRNA-dense regions and extracting  
46 gene expression profiles for each cell (i.e. local maxima) as the averaged gene expression in that unit  
47 area. *Qian X. et al.* [11], instead, proposed a probabilistic framework for jointly assigning mRNAs to  
48 segmented cells and cells to cell types based on scRNA-seq cell-type priors, achieving a fine  
49 classification of interneurons subtypes of CA1 hippocampal region.

50  
51 Despite these efforts for improving cell type identification in situ, spatial cell type analyses alone do  
52 not use the full power of in situ spatial transcriptomics: The subcellular resolution can reveal spatial  
53 heterogeneity also at subcellular levels. There is compelling evidence that many genes are expressed  
54 in a spatially dependent fashion independent of cell types [12], and this information is lost when  
55 analysing transcriptional profiles of single cells. Moreover, there is a considerable amount of

56 heterogeneity within each cell type explained by the balance between intrinsic regulatory networks  
57 and extrinsic subcellular processes depending on the local cellular microenvironment [13-17]. mRNA  
58 localization plays an important role in these cell differentiation processes as localization can vary  
59 during specific stages of cell development, and distinguishes cell phenotypes, activities and  
60 communication. Specifically, mRNA localization is involved in cellular compartmentalization of gene  
61 expression into spatial functional domains involved in spatially targeted segregation of protein  
62 synthesis [18]. For example, mRNA localization is particularly diffused in neurons, where protein  
63 synthesis can take place at distal sites far away from the nucleus: Dendritic and axonal structures  
64 express several forms of plasticity that requires local translation [19-22]. Disruption of these  
65 subcellular biological processes were shown to be implicated in neurodevelopmental, psychiatric or  
66 degenerative diseases [23-26]. It is thus important to take advantage of in situ mRNA detection  
67 methods to dissect the spatial heterogeneity of gene expression at subcellular resolution with respect  
68 to development and disease, and unveil the subcellular spatial domains underlying cell  
69 differentiation.

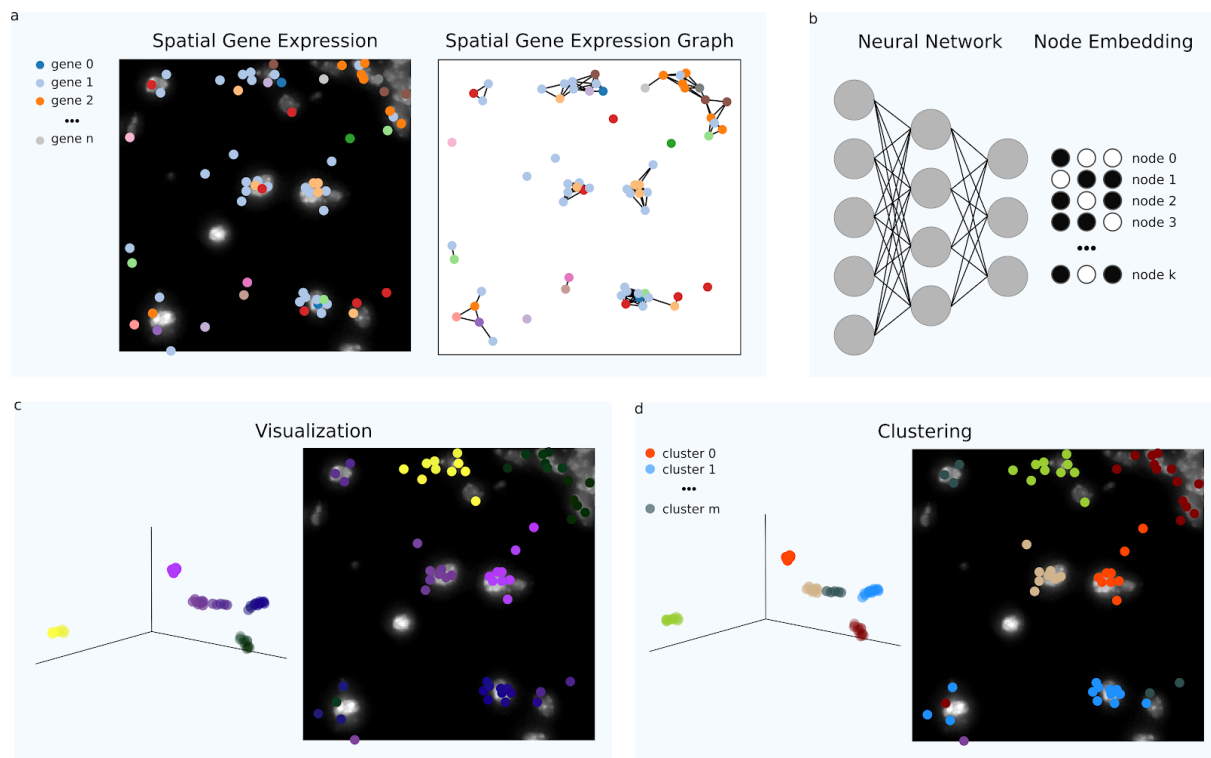
70

71 Here we propose a novel segmentation free approach for analyzing the spatial heterogeneity in gene  
72 expression of tissue samples that does not rely on the definition of cell types and cell segmentation  
73 but leverages the spatial organization of single mRNAs to define subcellular spatial domains involved  
74 in cellular differentiation. Specifically, we consider the spatial organization of mRNAs inside tissues as  
75 a spatial functional network where different mRNA types interact based on their spatial proximity  
76 [Figure 1], and where subcellular domains can be identified as clusters of local gene constellations  
77 that are shared or cell-type specific. In order to investigate the spatial mRNA network for recurrent  
78 gene constellations, we adopted a powerful graph representation learning technique [27] based on  
79 graph neural networks (GNN) [28], that has recently emerged as state-of-the-art machine learning  
80 technique for leveraging information from graph local neighborhoods. Therefore, each mRNA location  
81 is encoded in a graph as a node with a single feature representing the gene it belongs to and it is  
82 connected to all the other nodes representing the other mRNAs located in its neighborhood [Figure  
83 1a]. During training, the GNN learns the topological structure of each node's local neighborhood as  
84 well as the distribution of node features in the neighborhood (i.e. local gene expression), and projects

85 each node in a lower dimensional embedding space that encapsulates high-dimensional information  
86 about the node's neighborhood [Figure 1b]. We call this vectorization approach spatial gene  
87 expression to vector, or spage2vec, where geometric relations in this lower dimensional space  
88 corresponds to higher order relationships in the local gene environment. We apply spage2vec to three  
89 publicly available datasets and compare the resulting gene constellations to cell type maps presented  
90 in the respective publications.

91

92



93 **Figure 1.** Spage2vec workflow for detecting subcellular spatial domains from spatial gene expression data. (a) Spatial  
94 transcript locations of  $n$  targeted genes are encoded in a graph connecting neighboring mRNA spots based on their spatial  
95 distances. (b) A lower dimensional representation is learnt for each of the  $k$  mRNA spots using a graph representation learning  
96 technique based on a graph neural network. The neural network predicts a node embedding vector for each mRNA of the graph  
97 representing high order spatial relationships with its local neighborhood (Materials & Method). Thereafter, the spatial gene  
98 expression variation can be (c) visualized at subcellular resolution projecting the learnt node embedding vectors in RGB color  
99 space, or (d) unsupervised clustering analysis can define  $m$  different clusters representing distinct subcellular spatial functional  
100 domains.

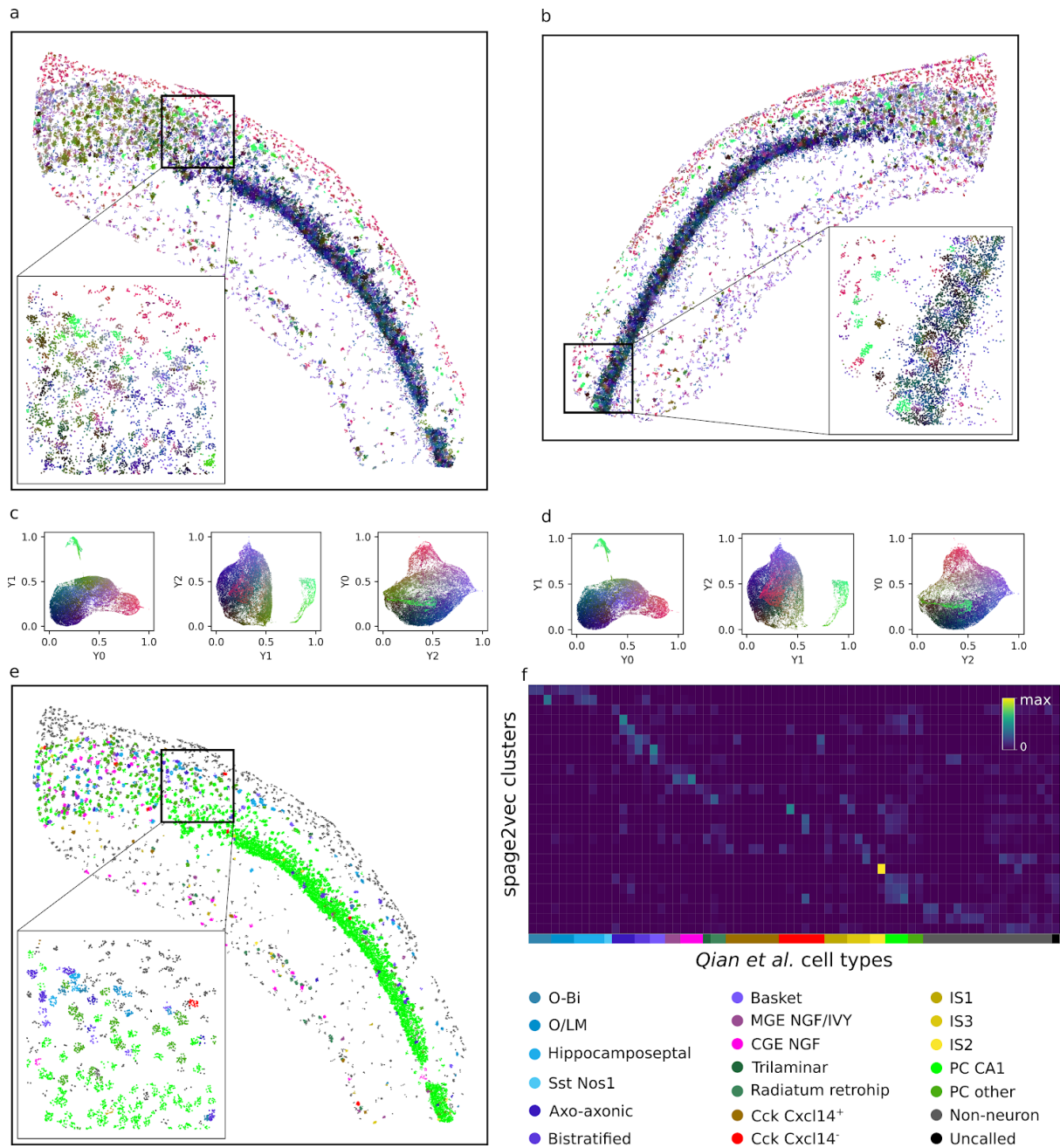
101

102 RESULTS

103 *Spage2vec for in situ sequencing analysis*

104 We first analyzed published in situ sequencing (ISS) data of mouse hippocampal area CA1 [11],  
105 where transcripts of 99 genes were localized. After representing the spatial gene expression as a  
106 graph, we applied spage2vec to generate a 50 dimensional embedding for each mRNA spot (Material  
107 & Methods), encoding information of its local neighborhood. We then projected the 50 dimensional  
108 embedding to three dimensions in order to visualize spatial relationships learnt from the data as  
109 similar colors in RGB color space [Figure 2a,c]. Next, in order to investigate if the learnt lower  
110 dimensional embedding contains significant information of biological functional domains, we clustered  
111 the spot embeddings directly in the 50-dimensional space (Material & Methods) and compared  
112 obtained spot cluster labels with cell-type annotations of spots from *Qian X. et al.* We initially obtained  
113 29 clusters [Figure 2 supplementary 1], which reduced to 25 after merging highly correlated clusters  
114 (Material & Methods). Identified clusters can be interactively explored at  
115 [https://tissuumaps.research.it.uu.se/demo/ISS\\_Qian\\_et\\_al.html](https://tissuumaps.research.it.uu.se/demo/ISS_Qian_et_al.html) [Supplementary File 1]. We then  
116 compared the 25 identified clusters with 20 cell-type- and 69 subcell-type-annotations defined in *Qian*  
117 *X. et al.*, excluding spots without cell-type labels [Figure 2e-f]. To demonstrate the ability of the model  
118 to generalize over unseen data, we used the spage2vec model trained on the right hemisphere  
119 mouse hippocampal area CA1 to predict the node embedding for the spatial gene expression graph of  
120 the left hemisphere CA1 area unseen during training [Figure 2b,d]. As can be seen in the figures  
121 [Figure 2a-d], the node representation of the two spatial gene expression graphs projected and  
122 visualized in RGB color space shows that the model produces visually similar embeddings for data  
123 not available during training.

124



125 **Figure 2.** Application of spage2vec to in situ sequencing data of mouse hippocampal area CA1. Visualization of functional  
 126 variation of spatial gene expression at subcellular resolution in right (a) and left (b) hippocampal area CA1 color coded based  
 127 on their node embedding projections in RGB color space for right (c) and left (d) hemisphere. (e) Spatial gene expression with  
 128 colored cell-type labels from Qian X. et al. analysis. (f) Heatmap showing the obtained spage2vec clusters with respect to cell-  
 129 and subcell-type annotations (marked with different colors) from Qian X. et al., and cell-type legend.

130

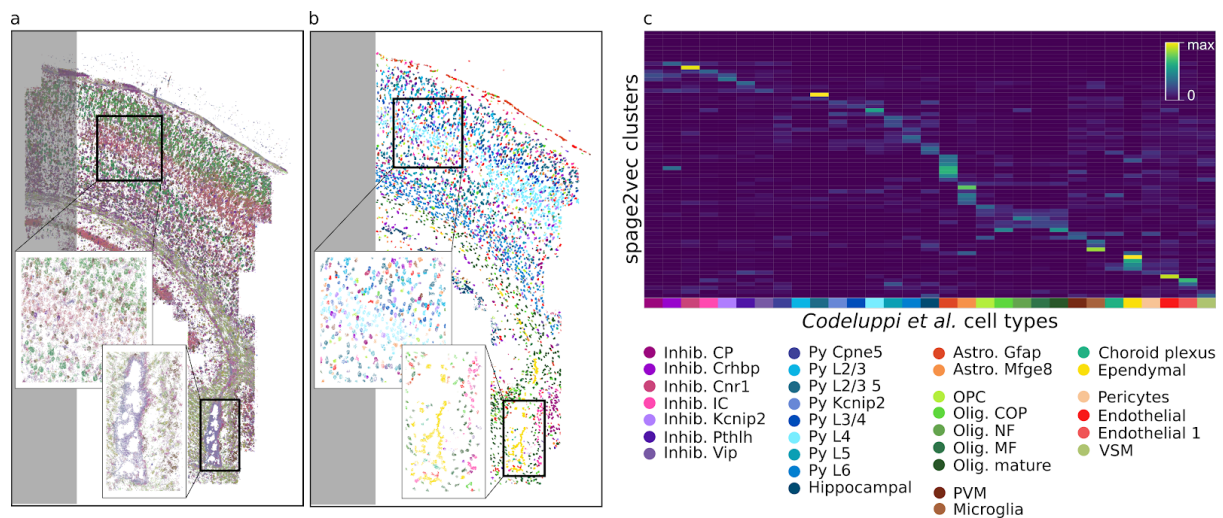
131 *spage2vec for osmFISH analysis*

132 In order to demonstrate the generalizability of spage2vec to other datasets, we also produced a lower  
 133 dimensional representation of mRNAs from published osmFISH data of 33 cell-type marker genes

134 targeted in mouse brain somatosensory cortex [7]. Again, we represented the gene expression as a  
135 graph and applied *spage2vec*, resulting in a 50 dimensional representation of each mRNA spot. We  
136 projected the 50 dimensions to three dimensions and visualized similar gene constellations as similar  
137 colors in 3D RGB color space [Figure 3a]. Next, we clustered the learnt embedding space in 274  
138 domains [Figure 3 supplementary 1], and reduced to 69 domains after merging highly correlated  
139 clusters (Material & Methods). Identified clusters can be interactively explored at  
140 [https://tissuumaps.research.it.uu.se/demo/osmFISH\\_Codeluppi\\_et\\_al.html](https://tissuumaps.research.it.uu.se/demo/osmFISH_Codeluppi_et_al.html) [Supplementary File 1].  
141 We then compared the resulting 69 clusters with the 31 cell-type annotations defined in *Codeluppi et al.*  
142 *al.*, excluding spots without cell-type labels [Figure 3b,c].

143

144



145 **Figure 3.** Application of *spage2vec* to osmFISH data from the mouse brain somatosensory cortex. (a) Visualization of  
146 functional variation of spatial gene expression at subcellular resolution color coded based on node embedding projection in  
147 RGB color space, and (b) spatial gene expression with colored cell-type labels from *Codeluppi S. et al.* cell segmentation.  
148 Shaded areas correspond to regions excluded in the original cell-type analysis. (c) Heatmap showing the obtained *spage2vec*  
149 clusters with respect to cell-type (marked with different colors) annotations from *Codeluppi S. et al.*, and cell-type legend.

150

### 151 *Spage2vec* for MERFISH analysis

152 We further applied *spage2vec* to a 3D mRNA localization dataset of hypothalamic preoptic region  
153 analyzed by MERFISH [6], where the transcripts of 135 targeted genes were localized in 3D. As for  
154 the previous dataset, we applied *spage2vec* to the graph representation (in this case 3D), and  
155 projected the 50 dimensions into three for visualization [Figure 4a]. Leveraging the symmetry of the

156 data we trained a spage2vec model on approximately half the sample (0-956  $\mu\text{m}$ ) and tested on the  
157 other half. Clustering in 50-dimensional space resulted in 198 clusters [Figure 4 Supplementary 1],  
158 which reduced to 121 after merging of clusters with a gene expression correlation greater than 95%.  
159 Identified clusters can be interactively explored at  
160 [https://tissuumaps.research.it.uu.se/demo/MERFISH\\_Moffitt\\_et\\_al.html](https://tissuumaps.research.it.uu.se/demo/MERFISH_Moffitt_et_al.html) [Supplementary File 1].  
161 We compared the gene expression profiles of these 121 clusters with the 10 cell-types and 76  
162 subcell-types presented in [6] [Figure 4b-d].

163

## 164 DISCUSSION

165 We showed that spage2vec can learn low dimensional embeddings encoding important topological  
166 and functional information of local gene expression. This rich low dimensional space can be used for  
167 downstream clustering analysis in order to detect biologically meaningful re-occurring gene  
168 constellations that correlate well with subcellular and cellular domains. The embedding, found by  
169 unsupervised training, has an inductive property to generalize over unseen nodes. This means that it  
170 can be applied to a new unseen dataset, as long as the new dataset has the same feature set (e.i.,  
171 consists of gene expression data from the same gene panel). This is especially useful to predict  
172 embeddings for new spatial gene expression datasets and map them to a common lower dimensional  
173 space. The fact that spage2vec is a fully unsupervised approach triggers the possibility for the  
174 discovery of novel cell-types in situ without the need of scRNA sequencing data driven analysis.

175

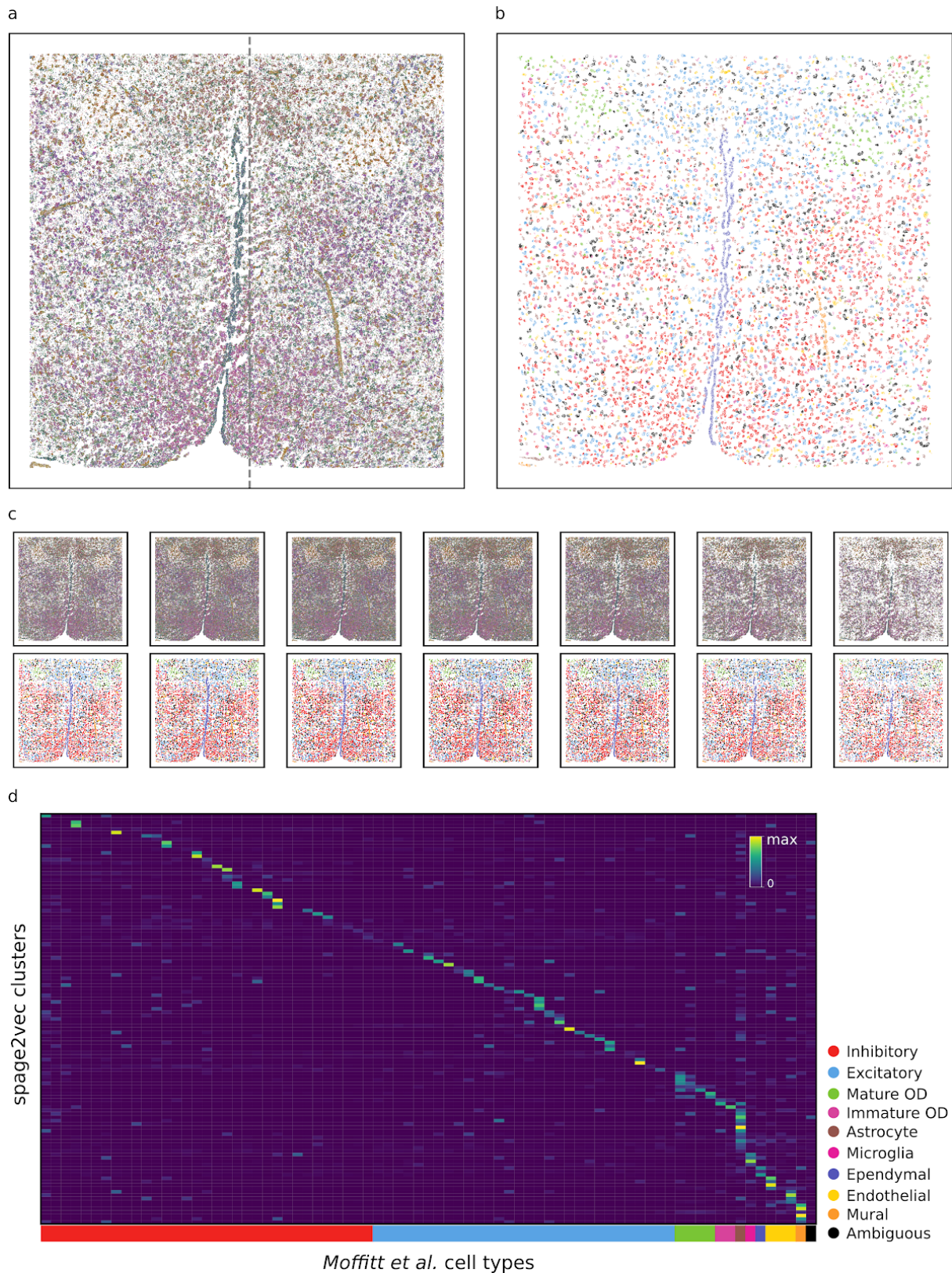
176 The presented approach is completely independent of cell segmentation, and equally applicable to 2D  
177 and 3D data, meaning that dense gene expression datasets such as those from MEHRFISH can be  
178 analyzed without relying on the accuracy of cell segmentation. In fact, most cell segmentation  
179 approaches are based on identifying cell nuclei, and then approximating gene-to-cell assignment by  
180 shortest distance to the closest nucleus. This can very often introduce noise as cells may vary very  
181 much in shape, and the nucleus of a given cell may not even be present in the same tissue section as  
182 the bulk of the cell. Furthermore, the presented segmentation free spage2vec approach enables



183 detection of cell types with varying sub-cellular gene expression patterns as well as subcellar  
184 constellations of genes representing functional domains located far away from a cell nucleus.

185

186



187 **Figure 4.** Application of spage2vec to MERFISH data of the mouse brain hypothalamic preoptic region. **(a)** Visualization of  
188 functional variation of spatial gene expression at subcellular resolution color coded based on their node embedding projections  
189 in RGB color space. The gray dashed line defines regions of the sample used for training (left) and for testing (right). **(b)** Spatial  
190 gene expression with colored cell-type labels from *Moffitt J. R. et al.* cell segmentation. **(c)** Spatial distribution of node  
191 embedding projections in RGB color space (upper row) and cell-type labels (bottom row) from *Moffitt J. R. et al.* across the  
192 whole section. **(f)** Heatmap showing the obtained spage2vec clusters with respect to cell- and subcell-type annotations (marked  
193 with different colors) from *Moffitt J. R. et al.*, and cell-type legend.

194

## 195 MATERIAL & METHODS

### 196 *Building a Spatial Gene Expression Graph*

197 Spatially resolved gene expression data consists of gene expression information and coordinates  
198 describing spatial location (in 2D or 3D) in a tissue sample. This information can be represented as a  
199 graph by saying that a node in the graph has a single categorical feature representing the gene  
200 expression (mRNA) it belongs to. Next, connections are drawn between each node and all its local  
201 neighbors within a maximum spatial distance  $d_{max}$ . The distance  $d_{max}$  is defined such that at least 97  
202 percent of all nodes are connected to at least one nearest neighbor, automatically adjusting for the  
203 spatial resolution of the dataset. Connected components with less than three nodes representing  
204 spurious expressions are removed from the graph before further processing [Figure 1a]. Note that the  
205 same graph representation works in both 2D and 3D.

206

### 207 *Neural Network Model and Training*

208 Next, spage2vec strives to transform the spatial gene expression graph into an embedding where  
209 similar gene constellations are assigned similar vectors using a neural network model. The neural  
210 network model consists of an unsupervised GraphSAGE [27] model implemented with the open  
211 source machine learning python library StellarGraph [29]. The model learns embeddings of unlabeled  
212 graph nodes by combining the node's own feature with features sampled and aggregated from the  
213 node's local neighborhood. Specifically, node embeddings are learnt by solving a binary node  
214 classification task that predicts whether arbitrary node pairs are likely to co-occur in a random walk  
215 performed on the graph. For this task the training set consists of *positive* node pairs, pairs that  
216 co-occur within walks of length 2 on the graph, and *negative* pairs of nodes uniformly randomly

217 selected from the graph. Through training this binary node pair classifier, the model automatically  
218 learns an inductive mapping from a high-dimensional feature space (i.e. spatial gene expression) to a  
219 lower dimensional node embedding space, describing gene constellations, preserving important  
220 topological and structural features of the nodes. The model architecture consists of two identical  
221 GraphSAGE encoder networks sharing weights, taking as input a pair of nodes together with the  
222 graph structure and producing as output a pair of node embeddings. Thereafter, a binary classification  
223 layer with a sigmoid activation function, learns to predict how likely it is that a pair will occur at a  
224 random position in the graph. Model parameters are optimized by minimizing binary cross-entropy  
225 between the predicted node pair labels and the true labels, without supervision.

226

### 227 *Neural network hyperparameters*

228 The proposed spage2vec model architecture used for all experiments presented here consists of two  
229 GraphSAGE layers with 50 hidden units, a bias term, l2 normalization, and l1 kernel regularization,  
230 using attentional aggregator function [30] with LeakyRelu [31]. Each GraphSAGE encoder embeds  
231 each node's neighborhood with a 2-hop node aggregation strategy, sampling respectively 20 and 10  
232 nodes for the first and the second hop. The model is trained with on-the-fly batch generation with  
233 batch size equal to 50, using Adam [32] as optimizer with learning rate equal to 0.5e-4. The output of  
234 spage2vec will thus be one vector of length 50 per spatial gene expression position. All details and  
235 settings are provided as Python notebooks (<https://github.com/wahlby-lab/spage2vec>).

236

### 237 *Visualization of node embeddings*

238 To visualize the extracted spatial gene expression embeddings created by spage2vec, we reduced  
239 the embedding dimensionality to three dimensions with UMAP [33]. This allowed us to present the  
240 spatial gene expression constellations as data points in a 3D RGB color space. Mapping the new  
241 color-coding back to tissue space shows that many of the constellations not only cluster in space but  
242 also seem to recur and correlate with cellular and subcellular spatial domains [Figure 1d].

243

244

245

## 246 *Identification of distinct gene constellations and spatial domains*

247 For further comparing the spage2vec output with approaches aimed at identifying cell types we  
248 hypothesize that recurring constellations of genes are spatial functional domains that may be cell type  
249 specific, or represent processes shared among different cell types. We therefore cluster the  
250 50-dimensional spage2vec output using the Leiden clustering algorithm [34,35] followed by Z-score  
251 normalization of the cluster expression matrix (cluster x genes). Clusters where gene expression  
252 counts have a correlation greater than 95% are merged, and the merged cluster expression matrix is  
253 re-normalized with Z-score normalization, leading to a final set of clusters. Note that the trained model  
254 has an inductive property, meaning that it can generalize and find embeddings for previously unseen  
255 gene constellations.

256

## 257 *Datasets*

258 We apply spage2vec to three publicly available published mouse brain tissue datasets obtained by  
259 three different spatial transcriptomics assays: (1) In situ sequencing (ISS) of left and right  
260 hippocampal area CA1 [11, [https://tissuomaps.research.it.uu.se/demo/ISS\\_Qian\\_et\\_al.html](https://tissuomaps.research.it.uu.se/demo/ISS_Qian_et_al.html)], with a  
261 resolution of 0.325  $\mu\text{m}$  per px and a total of 84880 detections of 99 different mRNAs. We refer to this  
262 as the ISS dataset. (2) An osmFISH analysis of the somatosensory cortex [7,  
263 [https://tissuomaps.research.it.uu.se/demo/osmFISH\\_Codeluppi\\_et\\_al.html](https://tissuomaps.research.it.uu.se/demo/osmFISH_Codeluppi_et_al.html)], comprising a tissue  
264 section of 3.8  $\text{mm}^2$ , with a resolution of 0.065  $\mu\text{m}$  per pixel, and a total of 1802589 detections of 33  
265 different mRNAs. We refer to this as the osmFISH dataset. (3) A MERFISH analysis of the  
266 hypothalamic preoptic region [6,  
267 [https://tissuomaps.research.it.uu.se/demo/MERFISH\\_Moffitt\\_et\\_al.html](https://tissuomaps.research.it.uu.se/demo/MERFISH_Moffitt_et_al.html)], comprising a 3D tissue  
268 section 10  $\mu\text{m}$  thick of 1.8 by 1.8 mm and a total of 3728169 detections targeting 135 different genes,  
269 referred to as the MERFISH dataset.

270

## 271 *Code Availability*

272 All software was developed in Python 3 using open source libraries. The processing pipeline and the  
273 source code used to generate figures and analysis results presented in this paper are available as  
274 Python notebooks at <https://github.com/wahlby-lab/spage2vec>.

275

## 276 ACKNOWLEDGMENTS

277 We thank Mats Nilsson, Sten Linnarsson and Xiaowei Zhuang for making their datasets publicly  
278 available. We also thank Leslie Solorzano for providing support in visualization of the results with the  
279 TissUUmaps viewer. This research was funded by the European Research Council via ERC  
280 Consolidator grant 682810 to C. Wählby and Swedish Foundation for Strategic Research (grant  
281 BD150008).

282

## 283 COMPETING INTERESTS

284 The authors have no competing interests.

285

## 286 REFERENCES

- 287 [1] Svensson, V., Vento-Tormo, R., & Teichmann, S. A. (2018). Exponential scaling of single-cell  
288 RNA-seq in the past decade. *Nature protocols*, 13(4), 599-604.
- 289 [2] Grün, D., & van Oudenaarden, A. (2015). Design and analysis of single-cell sequencing  
290 experiments. *Cell*, 163(4), 799-810.
- 291 [3] Regev, A., Teichmann, S. A., Lander, E. S., Amit, I., Benoist, C., Birney, E., ... & Clevers, H. (2017).  
292 Science forum: the human cell atlas. *Elife*, 6, e27041.
- 293 [4] Shah, S., Lubeck, E., Zhou, W., & Cai, L. (2016). In situ transcription profiling of single cells reveals  
294 spatial organization of cells in the mouse hippocampus. *Neuron*, 92(2), 342-357.
- 295 [5] Wang, X., Allen, W. E., Wright, M. A., Sylwestrak, E. L., Samusik, N., Vesuna, S., ... & Nolan, G. P.  
296 (2018). Three-dimensional intact-tissue sequencing of single-cell transcriptional states. *Science*,  
297 361(6400), eaat5691.
- 298 [6] Moffitt, J. R., Bambah-Mukku, D., Eichhorn, S. W., Vaughn, E., Shekhar, K., Perez, J. D., ... &  
299 Zhuang, X. (2018). Molecular, spatial, and functional single-cell profiling of the hypothalamic preoptic  
300 region. *Science*, 362(6416), eaau5324.
- 301 [7] Codeluppi, S., Borm, L. E., Zeisel, A., La Manno, G., van Lunteren, J. A., Svensson, C. I., &  
302 Linnarsson, S. (2018). Spatial organization of the somatosensory cortex revealed by osmFISH.  
303 *Nature methods*, 15(11), 932-935.

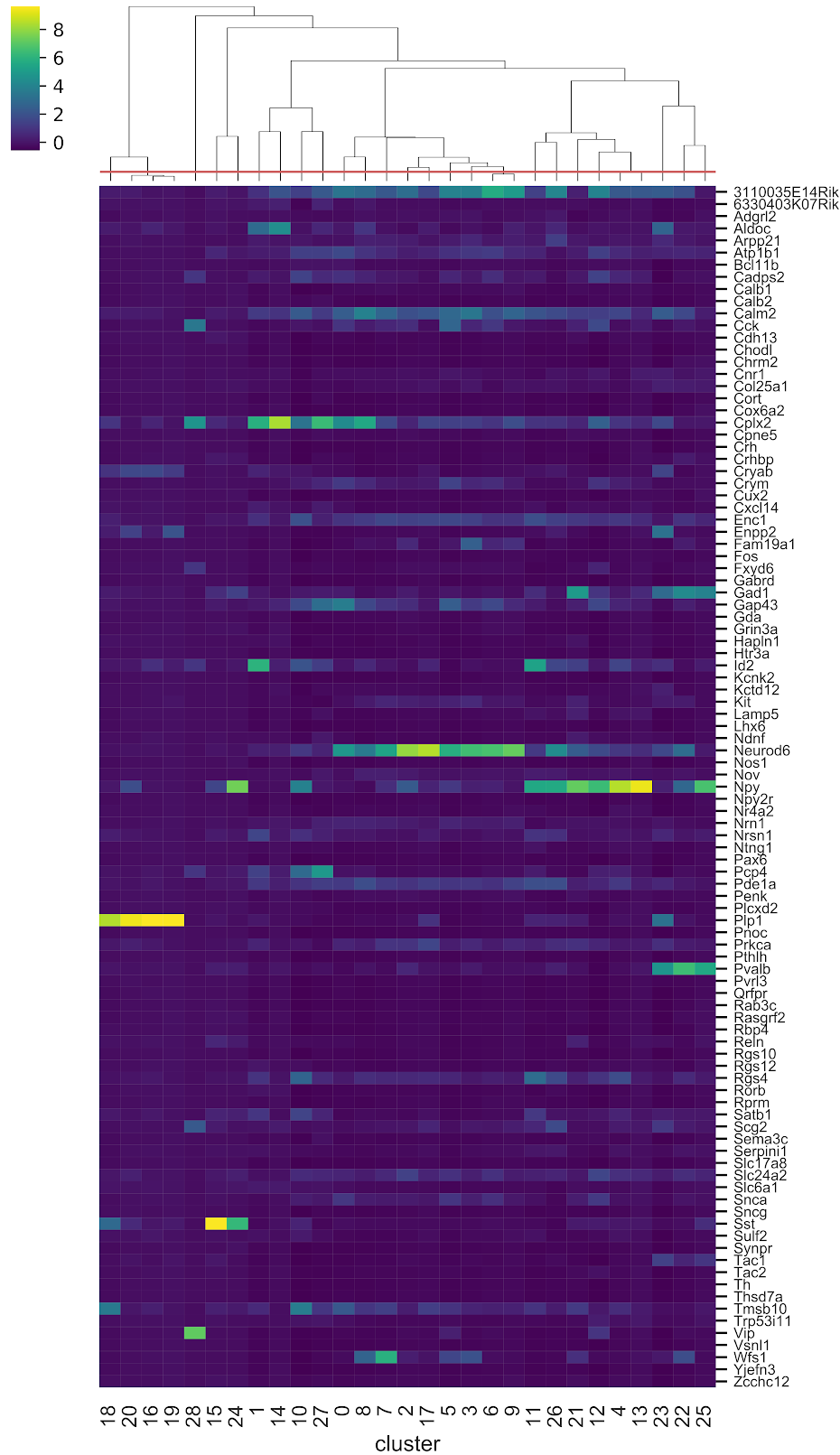
- 304 [8] Eng, C. H. L., Lawson, M., Zhu, Q., Dries, R., Koulena, N., Takei, Y., ... & Cai, L. (2019).  
305 Transcriptome-scale super-resolved imaging in tissues by RNA seqFISH+. *Nature*, 568(7751),  
306 235-239.
- 307 [9] Park, J., Choi, W., Tiesmeyer, S., Long, B., Borm, L. E., Garren, E., ... & Eils, R. (2019).  
308 Segmentation-free inference of cell types from in situ transcriptomics data. *bioRxiv*, 800748.
- 309 [10] Parzen, E. (1962). On estimation of a probability density function and mode. *The annals of*  
310 *mathematical statistics*, 33(3), 1065-1076.
- 311 [11] Qian, X., Harris, K. D., Hauling, T., Nicoloutsopoulos, D., Muñoz-Manchado, A. B., Skene, N., ... &  
312 Nilsson, M. (2020). Probabilistic cell typing enables fine mapping of closely related cell types in situ.  
313 *Nature methods*, 17(1), 101-106.
- 314 [12] Zhu, Q., Shah, S., Dries, R., Cai, L., & Yuan, G. C. (2018). Identification of spatially associated  
315 subpopulations by combining scRNAseq and sequential fluorescence in situ hybridization data.  
316 *Nature biotechnology*, 36(12), 1183.
- 317 [13] Quail, D. F., & Joyce, J. A. (2013). Microenvironmental regulation of tumor progression and  
318 metastasis. *Nature medicine*, 19(11), 1423.
- 319 [14] Riquelme, P. A., Drapeau, E., & Doetsch, F. (2008). Brain micro-ecologies: neural stem cell  
320 niches in the adult mammalian brain. *Philosophical Transactions of the Royal Society B: Biological*  
321 *Sciences*, 363(1489), 123-137.
- 322 [15] Swain, P. S., Elowitz, M. B., & Siggia, E. D. (2002). Intrinsic and extrinsic contributions to  
323 stochasticity in gene expression. *Proceedings of the National Academy of Sciences*, 99(20),  
324 12795-12800.
- 325 [16] Tirosh, I., Izar, B., Prakadan, S. M., Wadsworth, M. H., Treacy, D., Trombetta, J. J., ... &  
326 Fallahi-Sichani, M. (2016). Dissecting the multicellular ecosystem of metastatic melanoma by  
327 single-cell RNA-seq. *Science*, 352(6282), 189-196.
- 328 [17] Zhang, J., & Li, L. (2008). Stem cell niche: microenvironment and beyond. *Journal of Biological*  
329 *Chemistry*, 283(15), 9499-9503.
- 330 [18] Buxbaum, A. R., Haimovich, G., & Singer, R. H. (2015). In the right place at the right time:  
331 visualizing and understanding mRNA localization. *Nature reviews Molecular cell biology*, 16(2),  
332 95-109.

- 333 [19] Cajigas, I. J., Tushev, G., Will, T. J., tom Dieck, S., Fuerst, N., & Schuman, E. M. (2012). The  
334 local transcriptome in the synaptic neuropil revealed by deep sequencing and high-resolution imaging.  
335 *Neuron*, 74(3), 453-466.
- 336 [20] Besse, F., & Ephrussi, A. (2008). Translational control of localized mRNAs: restricting protein  
337 synthesis in space and time. *Nature reviews Molecular cell biology*, 9(12), 971-980.
- 338 [21] Holt, C. E., & Bullock, S. L. (2009). Subcellular mRNA localization in animal cells and why it  
339 matters. *Science*, 326(5957), 1212-1216.
- 340 [22] Das, S., Singer, R. H., & Yoon, Y. J. (2019). The travels of mRNAs in neurons: do they know  
341 where they are going?. *Current opinion in neurobiology*, 57, 110-116.
- 342 [23] Miller, S., Yasuda, M., Coats, J. K., Jones, Y., Martone, M. E., & Mayford, M. (2002). Disruption of  
343 dendritic translation of CaMKII $\alpha$  impairs stabilization of synaptic plasticity and memory consolidation.  
344 *Neuron*, 36(3), 507-519.
- 345 [24] Perry, R. B. T., Doron-Mandel, E., Iavnilovitch, E., Rishal, I., Dagan, S. Y., Tsoory, M., ... & Twiss,  
346 J. L. (2012). Subcellular knockout of importin  $\beta$ 1 perturbs axonal retrograde signaling. *Neuron*, 75(2),  
347 294-305.
- 348 [25] Yoon, B. C., Jung, H., Dwivedy, A., O'Hare, C. M., Zivraj, K. H., & Holt, C. E. (2012). Local  
349 translation of extranuclear lamin B promotes axon maintenance. *Cell*, 148(4), 752-764.
- 350 [26] Swanger, S. A., & Bassell, G. J. (2011). Making and breaking synapses through local mRNA  
351 regulation. *Current opinion in genetics & development*, 21(4), 414-421.
- 352 [27] Hamilton, W., Ying, Z., & Leskovec, J. (2017). Inductive representation learning on large graphs.  
353 In *Advances in neural information processing systems* (pp. 1024-1034).
- 354 [28] Wu, Z., Pan, S., Chen, F., Long, G., Zhang, C., & Yu, P. S. (2019). A comprehensive survey on  
355 graph neural networks. *arXiv preprint arXiv:1901.00596*.
- 356 [29] CSIRO's Data61. (2018). StellarGraph Machine Learning Library.  
357 <https://github.com/stellargraph/stellargraph>.
- 358 [30] Veličković, P., Cucurull, G., Casanova, A., Romero, A., Lio, P., & Bengio, Y. (2017). Graph  
359 attention networks. *arXiv preprint arXiv:1710.10903*.
- 360 [31] Maas, A. L., Hannun, A. Y., & Ng, A. Y. (2013, June). Rectifier nonlinearities improve neural  
361 network acoustic models. In *Proc. icml* (Vol. 30, No. 1, p. 3).

- 362 [32] Kingma, D. P., & Ba, J. (2014). Adam: A method for stochastic optimization. arXiv preprint  
363 arXiv:1412.6980.
- 364 [33] McInnes, L., Healy, J., & Melville, J. (2018). Umap: Uniform manifold approximation and  
365 projection for dimension reduction. arXiv preprint arXiv:1802.03426.
- 366 [34] Traag, V. A., Waltman, L., & van Eck, N. J. (2019). From Louvain to Leiden: guaranteeing  
367 well-connected communities. *Scientific reports*, 9(1), 1-12.
- 368 [35] Wolf, F. A., Angerer, P., & Theis, F. J. (2018). SCANPY: large-scale single-cell gene expression  
369 data analysis. *Genome biology*, 19(1), 15.

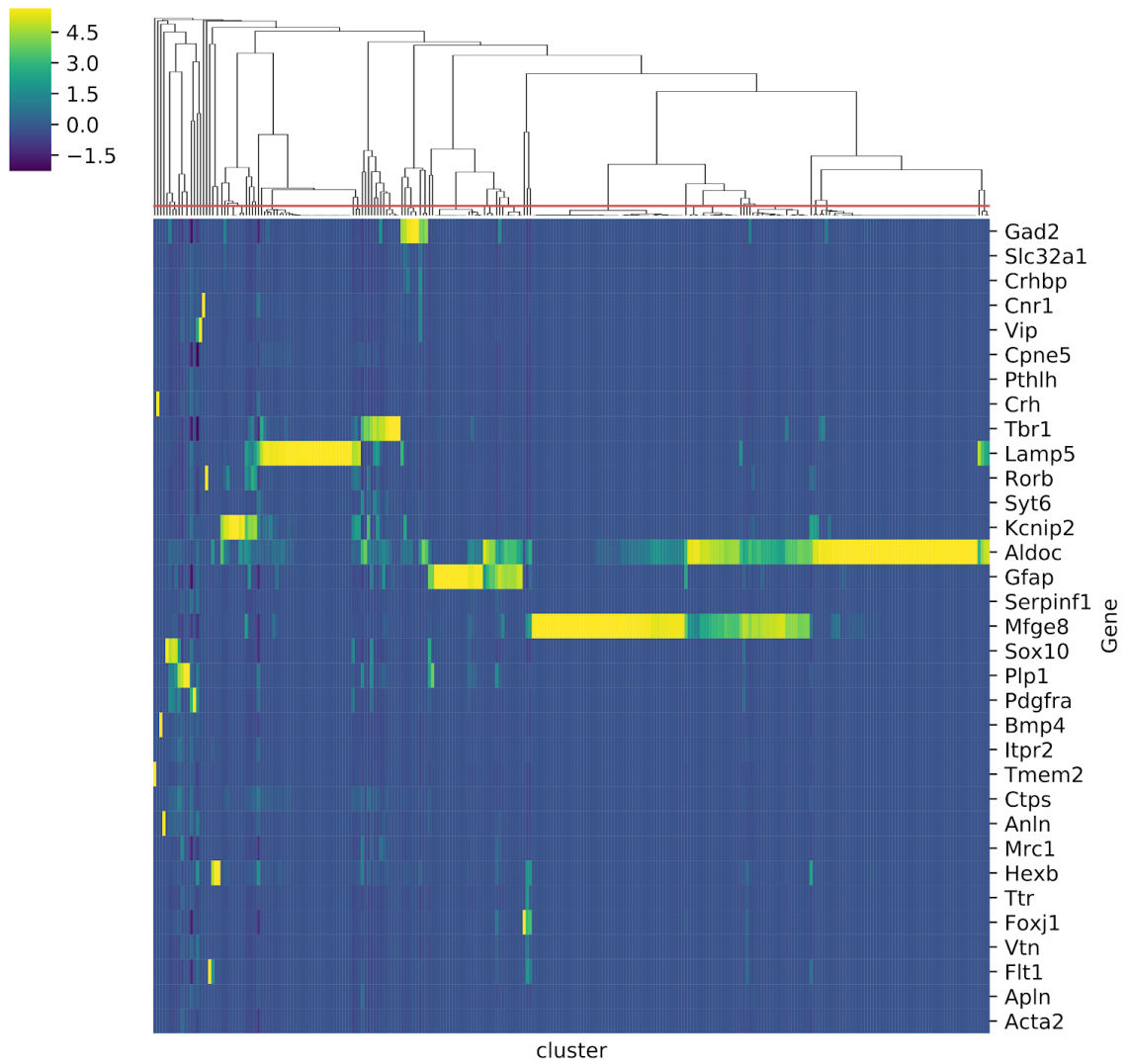


370



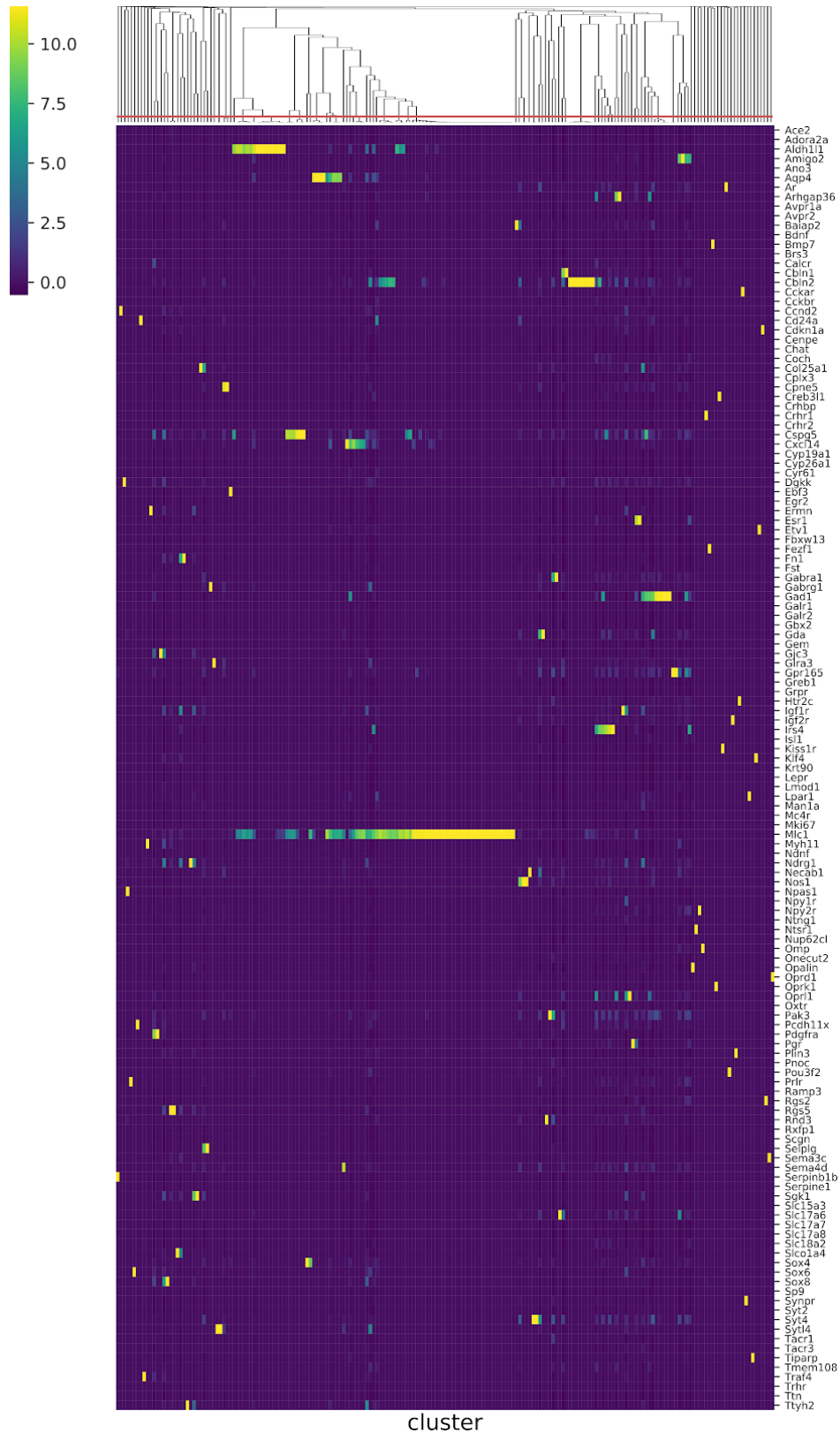
371 **Figure 2 supplement 1.** Gene expression per detected cluster, or gene constellation. Each column represents a cluster from  
 372 the spage2vec embedding of the ISS data from *Qian X. et al.* and each row shows how much each gene contributes to a given  
 373 cluster with Z-score normalized values. The red line on top of the dendrogram shows the correlation threshold used for merging  
 374 clusters.

375



376 **Figure 3 supplement 1.** Gene expression per detected cluster, or gene constellation. Each column represents a cluster from  
377 the spage2vec embedding of the osmFISH data from *CodeLuppi S. et al.*, and each row shows how much each gene  
378 contributes to a given cluster with Z-score normalized values. The red line on top of the dendrogram shows the correlation  
379 threshold used for merging clusters.

380



381 **Figure 3 supplement 1.** Gene expression per detected cluster, or gene constellation. Each column represents a cluster from  
382 the spage2vec embedding of the MERFISH data from *Moffitt J.R. et al.*, and each row shows how much each gene contributes  
383 to a given cluster with Z-score normalized values. The red line on top of the dendrogram shows the correlation threshold used  
384 for merging clusters.

385 SUPPLEMENTARY FILE 1

386

387 **Visualization of space2vec clusters in TissUMaps online viewer**

- 388 1. Open in a browser one of the following websites:
- 389     ○ ISS dataset:
- 390         [https://tissuomaps.research.it.uu.se/demo/ISS\\_Qian\\_et\\_al.html](https://tissuomaps.research.it.uu.se/demo/ISS_Qian_et_al.html)
- 391     ○ osmFISH dataset:
- 392         [https://tissuomaps.research.it.uu.se/demo/osmFISH\\_Codeluppi\\_et\\_al.html](https://tissuomaps.research.it.uu.se/demo/osmFISH_Codeluppi_et_al.html)
- 393     ○ MERFISH dataset:
- 394         [https://tissuomaps.research.it.uu.se/demo/MERFISH\\_Moffitt\\_et\\_al.html](https://tissuomaps.research.it.uu.se/demo/MERFISH_Moffitt_et_al.html)
- 395 2. Click on *Download data* in *Marker data* -> *Gene expression* tab, analysis results will
- 396 load in your browser.
- 397 3. Select “*macro\_cluster*” from *cluster column* drop down menu
- 398 4. Select “*global\_X\_pos*” from *X column* drop down menu
- 399 5. Select “*global\_Y\_pos*” from *Y column* drop down menu
- 400 6. Click on *Load markers*, the list of clusters with read counts , color and marker shape will
- 401 appear.
- 402 7. Check the *Show* box of the clusters you wish to visualize
- 403 *Note: For efficient visualization at the lower magnifications only a fraction of reads will be*
- 404 *displayed, while the number of displayed markers will increase zooming in to the highest*
- 405 *magnification (displaying all markers in the field of view).*
- 406 8. Marker size can be changed in *Global size* box for all the markers or in the *size* box for
- 407 the individual marker, as well as marker color and shape. Zooming in or out will refresh the
- 408 view and the update will be in place.